

# Design of biocompatible films with controllable properties and morphology through specific polypeptide/surfactant interactions

Javier Carrascosa-Tejedor,<sup>1,2\*</sup> Laura M. Miñarro,<sup>1</sup> Marina Efstratiou,<sup>2</sup> Imre Varga,<sup>3</sup> Maximilian W. A. Skoda,<sup>4</sup> Philipp Gutfreund,<sup>1</sup> Armando Maestro,<sup>5,6</sup> M. Jayne Lawrence<sup>2\*</sup> and Richard A. Campbell<sup>2\*</sup>

1. Institut Laue-Langevin, 71 Avenue des Martyrs, CS20156, 38042 Grenoble, France
2. Division of Pharmacy and Optometry, Faculty of Biology, Medicine and Health, University of Manchester, Oxford Road, Manchester M13 9PT, UK
3. Institute of Chemistry, Eötvös Loránd University, 112, Budapest H-1518, Hungary
4. ISIS Neutron and Muon Source, Rutherford Appleton Laboratory, Harwell Campus, Didcot OX11 0QX, UK
5. Basque Foundation for Science, Plaza Euskadi 5, Bilbao, 48009, Spain
6. Centro de Física de Materiales (CSIC, UPV/EHU) - Materials Physics Center MPC, Paseo Manuel de Lardizabal 5, E-20018 San Sebastián, Spain.

\* corresponding authors: [carrascosa-tejedor@ill.fr](mailto:carrascosa-tejedor@ill.fr) / [jayne.lawrence@manchester.ac.uk](mailto:jayne.lawrence@manchester.ac.uk) / [richard.campbell@manchester.ac.uk](mailto:richard.campbell@manchester.ac.uk)

## Electronic Supporting Information

### 1. Neutron reflectivity fitting procedure

The neutron reflectometry (NR) full- $Q_z$  approach was used to resolve the structure of PLL/SDS films at a 4.5:1 compression ratio in 3 different isotopic contrasts. The three contrasts measured are important to get specific information about the structure of the film. The d-SDS/ACMW contrast is very sensitive to SDS molecules both in the surface monolayer and the extended structures (ESs). The h-SDS/D<sub>2</sub>O contrast provides a sensitive measurement of the amount of ESs, as the difference between the scattering length density (SLD) of SDS and the bulk is high. Thus, the penetration of h-SDS molecules into the D<sub>2</sub>O subphase causes a strong modulation of the reflectivity profile. Lastly, the d-SDS/D<sub>2</sub>O contrast is essential to determine the presence of PLL in the ESs. Here, the SDS molecules and the subphase have a similar SLD but it is very different from that of PLL.

The data analysis has been performed in the Motofit software package of Igor Pro.<sup>1</sup> The analysis followed the general procedure of co-refining fits of the data in different isotopic contrasts using a structural model with a minimum number of layers. The optimised model has 6 stratified layers: (1) SDS tails, (2) SDS headgroups with PLL and solvent, (3) PLL, (4) PLL/SDS ESs and solvent, (5) PLL, and (6) PLL/SDS ESs and solvent. The multilayer structure is shown schematically in Figure SI1. Each layer,  $i$ , is characterized by four parameters: the SLD ( $\rho_i$ ), the thickness ( $d_i$ ), the roughness and the solvent volume fraction ( $V_{f,solvent}$ ). Table SI1 shows the values of scattering length,  $b$ , molecular volume,  $V_m$ , and scattering length density,  $\rho$ , of SDS and PLL.

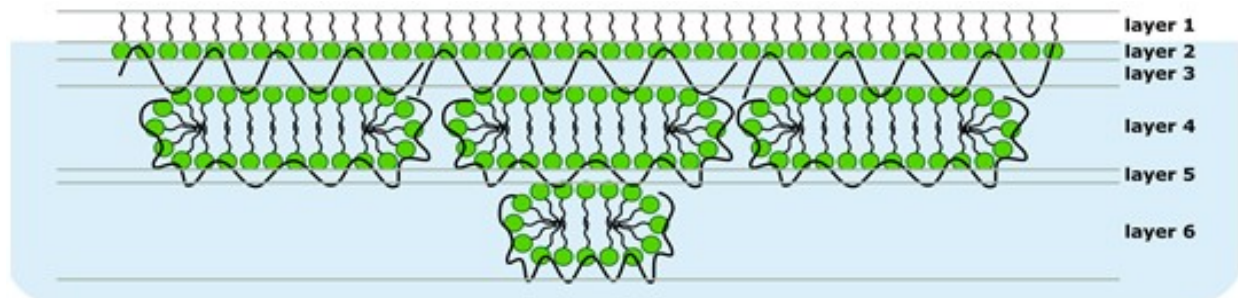


**Figure SI1.** Schematic representation of the multilayer structure used in the NR data analysis.

**Table SI1.** Scattering length ( $b$ ), molecular volume ( $V_m$ ) and scattering length density ( $\rho$ ) used in this work for the different components studied.

Component	$b$ (fm)	$V_m$ ( $\text{\AA}^3$ )	$\rho$ ( $\times 10^{-6} \text{\AA}^{-2}$ )
SS Headgroups	29.71	61	4.87
$C_{12}H_{25}$ -Chains	-13.76	352	-0.39
$C_{12}D_{25}$ -Chains	246.53	352	7.00
SDS Molecules	15.95	413	0.39
$d_{25}$ -SDS Molecules	276.24	413	6.69
PLL (in ACMW)	18.85	173	1.09
PLL (in $D_2O$ )	53.35	173	3.09

All interfaces were given a roughness of  $3.5 \text{\AA}$ , which is consistent with the presence of capillary waves.<sup>2</sup> All 'surface monolayer' (layers 1 and 2) parameters were fixed to those previously obtained with a 2:1 compression ratio,<sup>3</sup> as it was observed that the monolayer composition did not change after collapse, e.g., the thickness of the SDS tails was  $8.5 \text{\AA}$  as the SDS surface excess in the monolayer (i.e. the surfactant layer in contact with air with hydrated polyelectrolyte bound to the headgroups) equals  $4.0 \pm 0.1 \mu\text{mol}/\text{m}^2$ .<sup>2</sup> In the case of the headgroups layer (layer 2), there were two important constraints applied. First, the surface excess of tails and headgroups was constrained to be equal to ensure physical reality. Second, the SLD of the headgroups layer depended on the subphase used since PLL has labile protons in the amine groups that can exchange with the solution. We assumed 90% proton/deuterium exchange for PLL,<sup>4</sup> which translates into a headgroups SLD of  $1.09 \times 10^{-6} \text{\AA}^{-2}$  in ACMW and  $3.09 \times 10^{-6} \text{\AA}^{-2}$  in  $D_2O$ .

To minimise the number of free fitting parameters, a number of further model assumptions were made. First, the two layers of ESs were constrained to have the same thickness, given that they are each dominated by self-assembly of patches of SDS bilayer. Second, the same PLL/SDS stoichiometry as in the surfactant headgroups layer (layer 2) was used in the ESs (layers 4 and 6), i.e. 40% PLL. Third, as the solvent volume fraction of the PLL layers (layers 3 and 5) converged to zero in each preliminary fit, solvent was excluded in the optimised model. Five free fitting parameters remained:  $d$  of layers 3 (PLL), 5 (PLL) and 4 = 6 (ESs), and the solvent volume fraction,  $v_f$ , of layers 4 (ESs) and 6 (ESs). A genetic algorithm used, restricting fitting ranges of parameters to a physically meaningful values: 2–15 Å and 20–30 Å for the thicknesses of the PLL and ESs layers, respectively, with 0–1 for the two solvent volume fractions. Residual background values were used as follows:  $5 \times 10^{-6}$  for d-SDS in ACMW and  $3 \times 10^{-6}$  for d-SDS and h-SDS in D<sub>2</sub>O. The parameters used and fitted are shown in Table SI2. The uncertainties of the fitting parameters have been calculated as the difference between the optimised parameter and the variation of the optimised parameter that gives rise to an increase of the  $\chi^2$  of the fit by 10%.

**Table SI2.** Thickness ( $d_i$ ), scattering length density ( $\rho_i$ ), and composition obtained from the correspondent fit for each layer of the PLL/SDS films spread from overcharged aggregates, where  $i$  is the layer number.

Layer	Parameter	d-SDS/ACMW	d-SDS/D <sub>2</sub> O	h-SDS/D <sub>2</sub> O
1	$d_1$ (Å)	8.5		
	$\rho_1$ ( $\times 10^{-6}$ Å <sup>-2</sup> )	7	7	-0.39
	Composition	100% SDS chains		
2	$d_2$ (Å)	4		
	$\rho_2$ ( $\times 10^{-6}$ Å <sup>-2</sup> )	2.90	3.94	3.94
	Composition	37% SDS heads 40% PLL 23% solvent		
3	$d_3$ (Å)	12.0 ± 0.7		
	$\rho_3$ ( $\times 10^{-6}$ Å <sup>-2</sup> )	1.09	3.09	3.09
	Composition	100% PLL		
4	$d_4$ (Å)	26 ± 2		
	$\rho_4$ ( $\times 10^{-6}$ Å <sup>-2</sup> )	6.35	6.47	0.55
	Composition	73% SDS 5% PLL 22% solvent		
5	$d_5$ (Å)	3 ± 1		
	$\rho_5$ ( $\times 10^{-6}$ Å <sup>-2</sup> )	1.09	3.09	3.09
	Composition	100% PLL		
6	$d_6$ (Å)	26 ± 7		
	$\rho_6$ ( $\times 10^{-6}$ Å <sup>-2</sup> )	6.35	6.47	0.55
	Composition	9% SDS 1% PLL 90% solvent		

## 2. NR fitting demonstration of PLL between the ESs

Figure S12 shows the reflectivity profiles and fits using the optimised model (A) with and an alternative model (B) without PLL (layer 5) located between the two layers of ESs (layers 4 and 6). A fit of the data using the optimized model where the PLL layer is included between the ESs results in a  $\chi^2$  value of 18 (panel A), while the absence of this layer leads to a  $\chi^2$  of 25 (panel B), i.e. an increase of > 40% where the relative increase in number of free fitting parameters is 25%. In the case where the PLL layer is omitted, the model fit of the d-SDS/D<sub>2</sub>O contrast (i.e. the data most sensitive to the penetration of PLL beneath the surface monolayer) deviates strongly from the experimental data around the Kiessig fringe, emphasising the need for PLL to be included between the ESs. This result is also supported by the physical nature of oppositely charged polypeptide electrostatically screening the charges of the surfactant headgroups in the ESs.

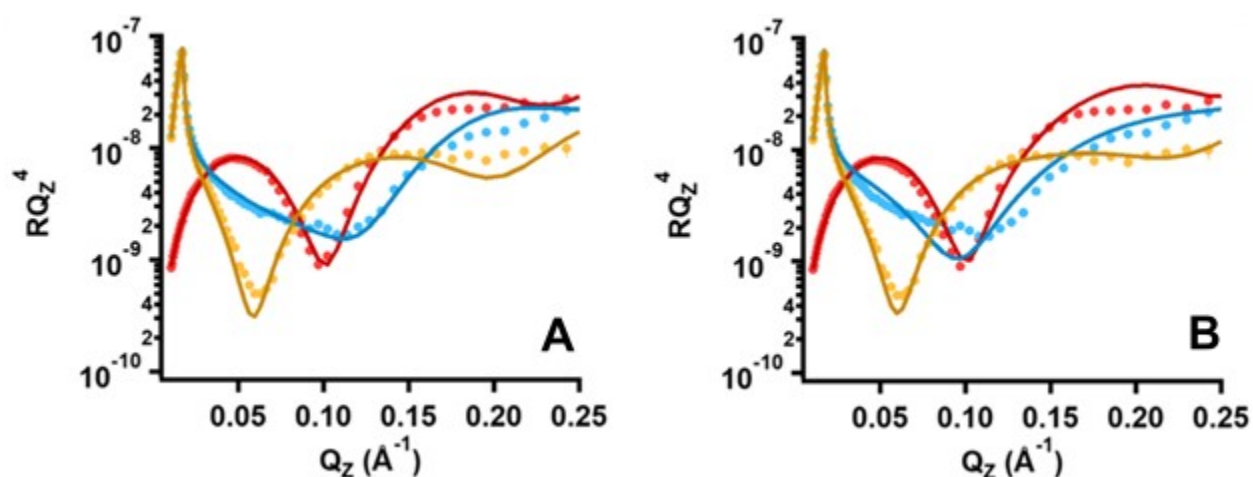


**Figure S12.** Neutron reflectivity profiles of a PLL/SDS film compressed to a 4.5:1 ratio using d-SDS/ACMW (red circles), d-SDS/D<sub>2</sub>O (blue circles) and h-SDS/D<sub>2</sub>O (orange circles) contrasts. The continuous lines show the fits using a model (A) with PLL between the ESs layers and (B) without PLL layer between the ESs layers.

## 3. Surface pressure and ellipsometry stability measurements

Ellipsometry was used to probe the stability of PLL/SDS and PLA/SDS films compressed to ratios of 2:1 and 5:1. These two compression ratios were chosen as the first is representative of the states of the films during the surface pressure collapse, and the second is representative of the states after the second kink in the isotherms where the apparent  $\Pi$  increases above  $\Pi_c$ . These experiments are considered insightful for assessing whether the films could be transferred to solids for future applications. The use of a technique such as Langmuir Blodgett/Schaefer would require films with the ESs to be stable for a period under optimal transfer conditions.

The experiments were performed by compressing the films at a constant speed until the maximum compression ratio was reached and the barriers were stopped. Both  $\Pi$  and  $d\Delta$  were

recorded during compression and for at least 1 h at maximum compression. Figures S13 and 4 shows the results obtained using a maximum compression ratio of 2:1 and 5:1, respectively. In all cases,  $\Pi$  relaxes after the barriers are stopped but  $d\Delta$  values remain stable indicating that the films presenting ESs that retain the excess of material are stable over long periods of time.

The high stability of the films makes it possible to determine their structure using NR. Such structural measurements usually lasts between 40 min and 1 h. Therefore, ellipsometry confirms that the amount of material present at the interface does not change during the NR measurement. Furthermore, the stability and the solid character of the films at high compression ratios indicates that they are suitable candidates for transfer to solid supports.

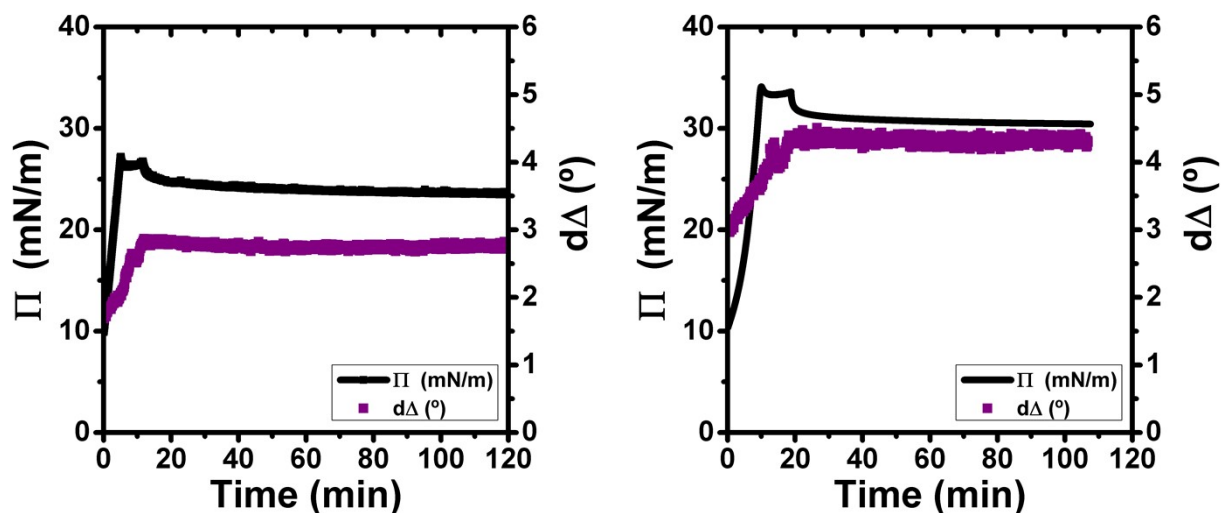


**Figure S13.** Variation of  $\Pi$  (black line) and  $d\Delta$  (purple diamonds) as a function of time of (A) PLL/SDS and (B) PLA/SDS spread films at a 2:1 compression ratio.

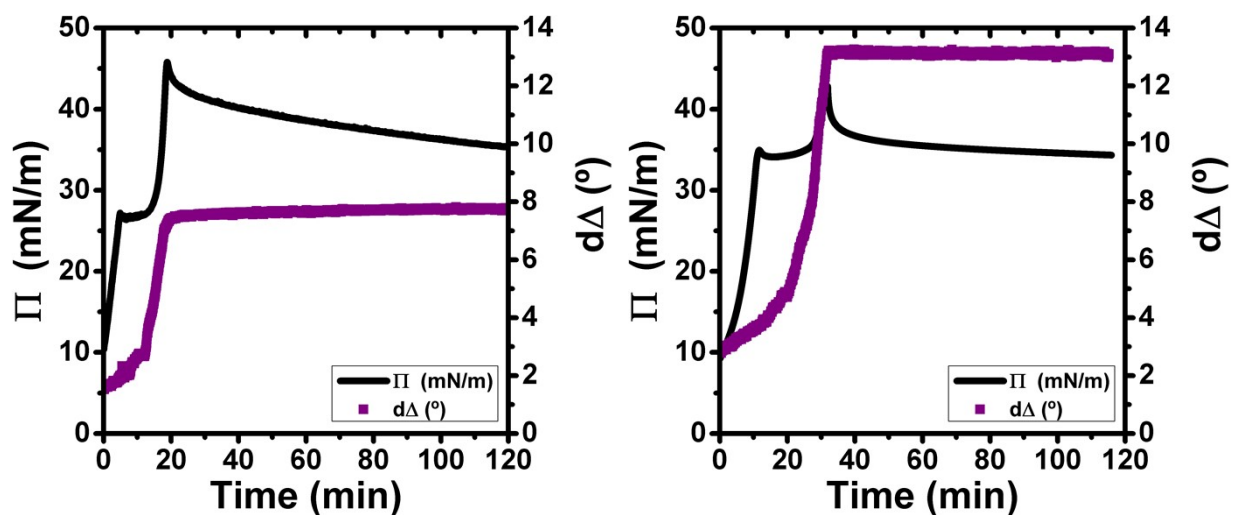


**Figure S14.** Variation of  $\Pi$  (black line) and  $d\Delta$  (purple diamonds) as a function of time of (A) PLL/SDS and (B) PLA/SDS spread films at a 5:1 compression ratio.

#### 4. Verification of surface pressure values at high compression ratios

Figure S15 shows data obtained in an experiment performed using 2 surface pressure sensors on PLL/SDS films with respect to compression of the surface area to a ratio of 10:1. The experiments were performed because of doubts over possible artefacts in measurements of  $\Pi$  that exceeded  $\Pi_c$  in case a phase transition of the film to a solid nature meant that the plate experienced an additional force from being pulled sideways during the compression process, and hence the values of  $\Pi$  no longer represented true surface pressure. Sensor 1 with a single plate was placed in contact with the film at the air/water interface and kept at the same position during the compression, while sensor 2 was repeatedly made to contact the film with a fresh plate each time while the barriers has briefly stopped the compression process. It was assumed that sensor 2 could not be affected by the possible artefact of the plate being pulled sideways. The approximately constant values obtained with sensor 2 after the collapse point indicates that the increase in surface pressure above  $\Pi_c$  is related to the additional force exerted by the solid film.

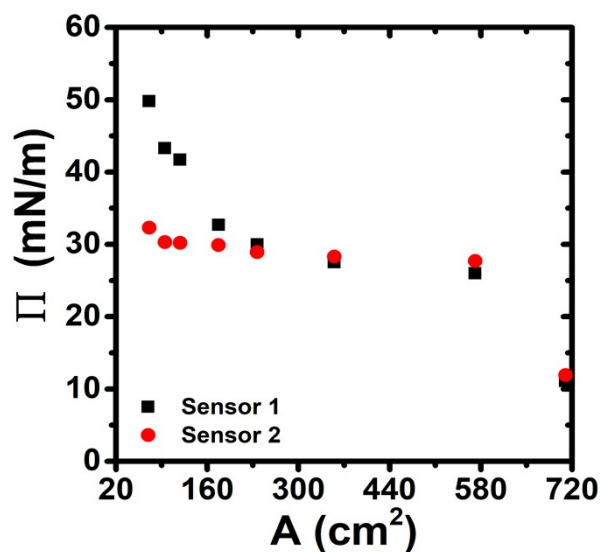


**Figure S15.** Variation of  $\Pi$  as a function of  $A$  using two different pressure sensors according to the methodology described in the text above.

#### References

1. A. Nelson. *J. Appl. Crystallogr.* **2006**, *39*, 273–276.
2. R. A. Campbell, Y. Saaka, Y. Shao, Y. Gerelli, R. Cubitt, E. Nazaruk, D. Matyszewska and M. J. Lawrence. *J. Colloid Interface Sci.* **2018**, *531*, 98–108.
3. J. Carrascosa-Tejedor, A. Santamaria, A. Tummino, I. Varga, M. Efstratiou, M. J. Lawrence, A. Maestro and R. A. Campbell. *Chem. Commun.* **2022**, *58*, 10687–10690.
4. B. Jacrot, B. Reports Prog. Phys. **1976**, *39*, 911–953.